CHEMISTRY OF MATERIALS

ARTICLE

pubs.acs.org/cm

Self-Standing Three-Dimensional Networks of Nanoparticles With Controllable Morphology by Dynamic Templating of Surfactant Hexagonal Domains

Kamendra P. Sharma,[†] Anal Kr. Ganai,[‡] Sayam Sen Gupta,[*,‡] and Guruswamy Kumaraswamy[*,†]

[†]Complex Fluids and Polymer Engineering, Polymer Science & Engineering Division, National Chemical Laboratory, Pune 411008, India

[‡]CReST Chemical Engineering Division, National Chemical Laboratory, Pune 411008, India

Supporting Information

ABSTRACT: Assembly of nanoparticles into free-standing three-dimensional networks has implications for a wide range of applications. We show that dynamic templating of surfactant hexagonal domains is a facile technique to organize nanoparticles into a network of particulate strands. Dispersed particles (>10 nm), independent of particle chemistry, assemble into networks, when the surfactant matrix cools into the hexagonal phase. We demonstrate assembly of inorganic, polymeric, and protein nanoparticles into networks. Where particle assembly is reversible, particles are coated with polymers that are subsequently cross-linked to stabilize the networks after surfactant removal. This technique involves near ambient temperatures and a benign water wash for template removal. The network mesh size can be varied from submicrometers to tens of micrometers by controlling the cooling rate. Particle networks can be flow-oriented prior to cross-linking, and interpenetrating networks can also be formed.

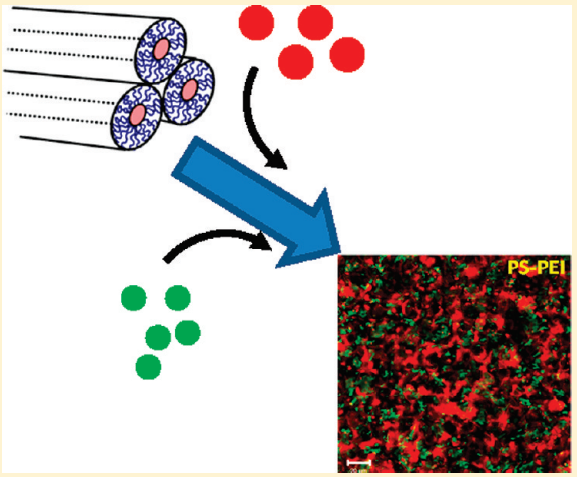

KEYWORDS: macroporous, nanoparticle, self-assembly, surfactant, hexagonal

INTRODUCTION

Assembly of nanoparticles into free-standing macroporous materials has implications for a wide range of technologically important applications, such as separation, chromatography, catalysis, filtration, insulation, and biomedical scaffolds. A variety of approaches have been demonstrated for nanoparticle assembly into macroporous materials,[1] including, spray drying,[2] polymer-induced aggregation,[3] controlled destabilization of nanoparticle dispersions,[4] and sol−gel assembly.[5] In these techniques, control over pore morphology is possible by optimization of processing parameters, but it is challenging. On the other hand, three-dimensional writing with nanoparticle inks[6] affords precise control over structure formation but is relatively complicated to implement.

An elegant strategy to create macroporous materials is to combine nanotectonics[7] (assembly of preformed nanoparticles), with templating of larger length scale structures,[8] including static templates, such as, colloidal crystals,[9] membranes,[10] gels,[11] polymer foams,[12] and biological organisms.[13] Nanoparticles can also be assembled around dynamic templates such as solvent drops in breath figures,[14] or in dynamic processing operations such as foaming.[15] In these methodologies, control over pore morphology remains a challenge and requires either preassembly of precisely defined templates or exquisite control over experimental protocols (viz. solvent condensation or foaming conditions). Recently, particles with specially tailored surface chemistry have been shown to segregate to interphases[16] and jam, thus arresting structural evolution in phase separating blends[17] to produce a percolated particulate assembly. There has also been renewed interest in dynamic templating of ice crystals by polymer−nanoparticle dispersions.[18] Ice templating allows control over pore size, shape, and orientation.[18] While ice templating is a powerful technique,[18] it involves freezing temperatures, and employs freeze-drying to remove the ice template. Thus, it would be advantageous to have a simpler technique to prepare macroporous materials using a wide variety of materials, that retains the elegance of ice templating, but employs milder conditions and involves easier template removal.

Templating of nematic domains, by particles expelled to domain boundaries, results in the formation of particulate networks.[19] This network formation is reversible, and the particles redisperse on heating above the liquid crystal clearing temperature;[19] thus, free-standing porous materials have not

Received: October 12, 2010
Revised: January 6, 2011
Published: February 22, 2011

been prepared using this route. Further, the particles need to be hydrophobic for dispersion in the liquid crystal, and network formation is observed only when impurities in the liquid crystal constrain the isotropic−nematic interface to propagate slowly.[19] In liquid crystal colloids with strong director anchoring, interactions between topological defects formed around dispersed particles result in particle organization.[20] Particles dispersed in lamellar phases segregate to defect nodes to stabilize "oily streak" networks.[21] However, none of the aforementioned techniques have been exploited to prepare macroporous materials.

Recently, we reported[22] a systematic study of the effect of particle size on their organization in a nonionic surfactant hexagonal (H_1) mesophase. Our results, in accord with the previous literature,[23] demonstrated that particles smaller than the characteristic H_1 spacing (spacing between surfactant assemblies, $a \approx 5$ nm) template the surfactant structure, while larger particles ($>\sim$10 nm) are expelled to form a network. For assembly of silica particles, network formation is rendered reversible[22] due to formation of micellar structures on the particle surface. However, interestingly, when the silica particles are coated with polyethyleneimine (PEI), it is observed that micelle-covered particle structures do not form.[24] Thus, PEI-coated particles can come into true physical contact, and cross-linking the PEI coat layer might enable us to stabilize the particulate networks.

Here, we demonstrate that dynamic templating of surfactant hexagonal domains is a facile technique to organize inorganic, organic, and biological nanoparticles into a network of particulate strands. This technique involves near ambient temperatures, and a benign water wash for template removal. The network mesh size can be varied from submicrometer to tens of micrometers by controlling the cooling rate, and networks can be flow-oriented.

EXPERIMENTAL SECTION

Materials. Ludox LS-30 silica particles (referred to as "Si") and nonionic surfactant, nonaethylene glycol monododecyl ether, $C_{12}E_9$ (characterized earlier[25]) were used as received from Sigma Aldrich. All other chemicals were used as obtained from Sigma Aldrich. Hydroxyapatite particles (HAP, Aldrich) were obtained as a 10 wt % dispersion in water and were sonicated using a probe sonicator immediately prior to coating with PEI (2000 g/mol). Fluorescent polystyrene latices were obtained from Microparticles GmbH, Germany.

Silica particles (90 nm diameter) were synthesized using the Stöber method. Amine groups were grafted onto these silica particles using a procedure reported earlier,[26] and finally, the particles were tagged with a fluorescent dye (FITC), as indicated in Schematic 1 and 2 in the Supporting Information. Details of the synthetic procedure can be found in the Supporting Information. The particles were characterized by transmission electron microscopy (TEM), thermogravimetric analysis (TGA), and infrared (IR). Poly(*N*-isopropylacrylamide) (PNIPAM) microgels[27] and positively charged magnetite (Fe_3O_4[28]) and ceria (CeO_2[29]) were prepared according to procedures reported in the literature and are described in detail in the Supporting Information. Particles without surface amine groups were coated with PEI using a modification of the reported method[30] (Supporting Information). PEI coated silica particles are referred to as Si-PEI.

General Methodology for Assembly of Nanoparticles for Making a Self-Standing Scaffold. Typically, a 10% (by weight) dispersion of nanoparticles was added to surfactant $C_{12}E_9$ at 50 °C, such that the surfactant to water ratio was 1:1. To this, glutaraldehyde was added, and then the solution was cooled to room temperature. Subsequently, sodium cyanoborohydride was added to the gel to reduce the imine groups formed upon cross-linking of PEI and glutaraldehyde. Finally, the scaffold was washed repeatedly with ethanol and water to remove the surfactant and afford the free-standing macroporous material.

For example, to form a macroporous solid from Si−PEI nanoparticles, the following procedure was followed. To 1000 mg of 10% (by weight) Si−PEI, 900 mg of $C_{12}E_9$ was added and homogenized in a water bath at 50 °C. At this temperature, 20 mg of glutaraldehyde (25 wt % solution) was added. The sample was then cooled to room temperature in a feedback controlled convective oven. The particle concentration in the overall composite is ∼5 wt %. The sample was then allowed to cross-link on standing at room temperature for a week. The sample was reacted with 0.1 M $NaCNBH_3$ solution and then (4−5 times) with water and ethanol to remove the surfactant. The silica scaffold was then dried in a vacuum oven at 120 °C before characterization. All the other particles were assembled and cross-linked by a similar procedure as mentioned above. Horse spleen ferritin did not require coating of PEI (due to presence of inherent amine functionalities) and was assembled in the H_1 phase as obtained from the supplier.

Material Characterization. Characterization of the particles/scaffolds was done using SAXS (Bruker Nanostar equipped with rotating anode and 2D wire detector, used over a q-range of 0.01−0.20 Å^{-1}). Samples were imaged using a Quanta 200 3D scanning electron microscope (SEM). Prior to SEM imaging, the sample was sputter coated using a Polaron SC 6420 sputter coater giving an Au thickness of 5 nm on the sample. An LSM 710 Carl Zeiss laser scanning confocal microscope (LSCM) was used to image the fluorescent samples. We used a He−Ne laser (543 nm) and an Argon-ion laser (488 and 514 nm) for our experiments. Zeta potential measurements were performed on a 90 Plus particle size analyzer (Brookhaven Instruments, USA). TEM measurements were done at 100 kV on an FEI Technai F30. Optical microscopy was performed using an Olympus-BX 50 equipped with a crossed polarizer setup.

RESULTS AND DISCUSSION

Network formation by PEI-coated silica particles proceeds in the same manner as previously described for the uncoated silica particles.[22] Above the H_1-isotropic transition temperature, $T_{HI} \approx$ 45 °C, 15 nm PEI-coated silica nanoparticles (Si−PEI, 5%, by weight) are well-dispersed in the isotropic micellar phase of a 50% aqueous solution of nonionic surfactant, $C_{12}E_9$. On cooling below T_{HI} (at 5 °C/min), the particles are expelled by growing H_1 domains.[22] Once the H_1 domains (observed as birefringent bright regions between crossed polarizers, Figure 1a) grow to impingement, the particles jam to form a network. A comparison of optical micrographs of this sample viewed between crossed (Figure 1a) and parallel polarizers (Figure 1b) shows that the H_1 phase boundaries are optically dense. In contrast, for an H_1 phase not containing silica particles, domain boundaries are not visible between parallel polarizers. Thus, segregation of silica particles to the H_1 domain boundaries results in the optical contrast observed in Figure 1b.

The bulk three-dimensional structure of the particle network formed can be visualized using confocal microscopy to image the structure formed by assembly of fluorescently tagged 90 nm silica particles in the H_1 phase (Supporting Information). Confocal microscopy confirms that a three-dimensional connected network is formed as the particles self-assemble into linear aggregates. A two-dimensional projection of the three-dimensional image is shown in Figure 1c. The formation of linear aggregates suggests that particles are localized specifically where multiple H_1 domains meet. A 2D slice of network structure (Supporting Information) shows that the particle organization is similar to

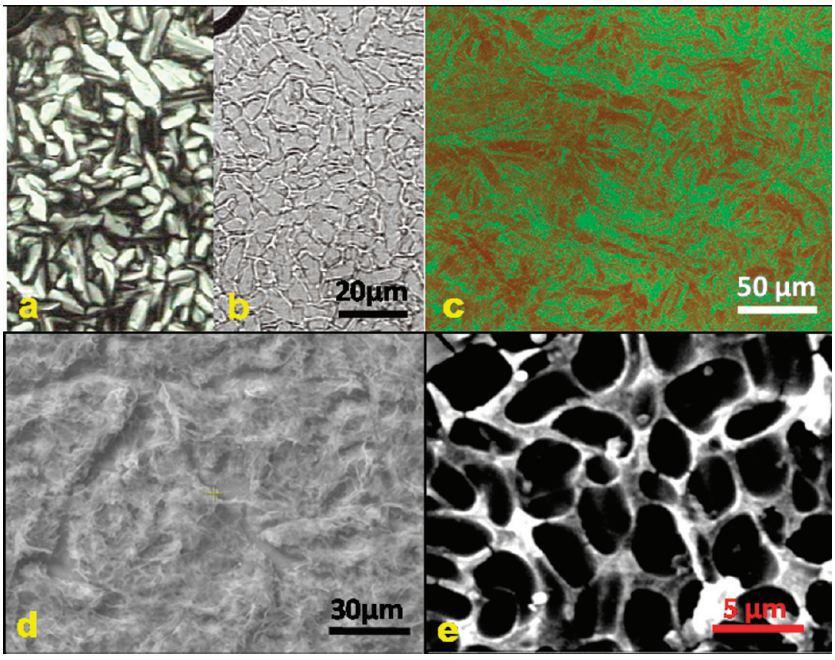

Figure 1. Optical microscopy of 5% (by weight) PEI-coated 15 nm silica particles in H_1 phase at room temperature (sample thickness $\approx 10\ \mu$m). The sample was cooled from isotropic phase at 50 °C to room temperature at 5 °C/min. (a) Between crossed polarizers, birefringent H_1 domains grown to impingement. (b) Same sample as part a, viewed between parallel polarizers. This shows that the boundaries of the H_1 domains are optically dense. In contrast, for an H_1 phase not containing silica particles, domain boundaries are not visible between parallel polarizers. Thus, segregation of the silica particles to the H_1 domain boundaries results in the optical contrast observed here. (c) Confocal microscope 2D projection image of 90 nm FITC-tagged Stöber silica particles in the H_1 phase. The sample is prepared by cooling the particle−surfactant−water system from 50 °C to room temperature at 5 °C/min. A red dye (DCM) is dispersed in the H_1 phase. Thus, we observe a network of fluorescent green silica particles in the red H_1 matrix. (d) SEM of a free-standing 3D scaffold prepared by cross-linking a network of PEI-coated 15 nm silica in the H_1 phase, (5 wt %) using glutaraldehyde. SEM is performed on a dry sample, after removal of the surfactant by washing. (e) Magnified section of the cross-linked scaffold.

that observed in optical micrographs on thinner samples (compare with Figure 1a).

Networks form for particles larger than about 10 nm (viz., greater than characteristic H_1 spacing, a = 5.6 nm, in these experiments). In practice, an upper bound for the size of particles that we can use to form networks is determined by particle sedimentation—we are unable to form networks from particles that are too large to stay dispersed as the surfactant solution is cooled ($\sim$1 μm for silica particles, $\sim$O(10 μm) for polystyrene particles). The nonionic surfactant H_1 phase in our experiments is characterized by an elastic constant, $K \sim$ O(1 pN), and we estimate that the anchoring strength of surfactant micelles on the particle surface is given by $W = k_BT/a^2 \approx 100\ \mu\text{J/m}^2$. For silica particles whose size, R, varies from 10 nm to 1 μm, the nondimensional ratio of anchoring and elastic energies, WR/K varies from $\sim$O(1) to $\sim$O(100). Thus, in our experiments, the director is strongly anchored to the particles and we expect deformation of the director field to govern long-range particle−particle interactions.[19,20] However, in our system, particle assembly appears to be governed primarily by expulsion of particles from the mesophase.

To stabilize the particulate network against dispersion after H_1 template removal, the PEI-coated silica particles were cross-linked with glutaraldehyde upon network formation. Subsequent to cross-linking, the surfactant could be readily removed by washing with water, to yield a free-standing particulate macroporous solid (Figure 1d). Scanning electron microscopy reveals a network structure (Figure 1d) comprised of a dense mesh of strands, with strand thickness varying from about 100 nm to a micrometer as seen at higher magnification (Figure 1e). Typically, scaffolds prepared using PEI-coated silica particles had an organic content of 12−13% (by weight). Macroscopic centimeter size samples of the macroporous materials were readily prepared (Supporting Information) and can be readily handled despite their high void fraction.

On cooling below T_{HI}, H_1 domains nucleate and grow[31] to impingement. Thus, by varying the nucleation density of H_1 domains, it is possible to vary the size of the domains and, therefore, the characteristic spacing of the particulate network. Fast cooling, for example at 10 °C/min (Figure 2a), results in particulate networks with smaller "strut" spacing as compared to cooling at 5 °C/min (Figure 2b and Figure 1a and b). As the sample is cooled at even slower cooling rates of 0.5 °C/min, the strut spacing increases (Figure 2c). Optical micrographs of networks formed by cross-linking Si−PEI reveal that the average mesh spacing can be varied from $\sim 3.1 \pm 0.7$ to $\sim 26.4 \pm 5.6\ \mu$m, on decreasing the cooling rate from 40 to 0.5 °C/min (Figure 2a−c and f, spacings obtained by averaging over at least 150 domains from optical micrographs taken at more than 10 separate locations; optical micrographs for samples cooled at 20 and 40 °C/min are in the Supporting Information). Freeze fracture TEM of rapidly cooled (>300 °C/min) samples indicate a mesh size of about $0.450 \pm 0.12\ \mu$m.[22] Thus, the mesh spacing can be varied by $\sim$50-fold, by simply controlling the cooling rate. The anisotropic shape of the particle-templated regions reflects the geometry of growing H_1 domains—in hexagonal mesophases, domains develop as elongated "bâtonnets",[32] before they grow into characteristic fan-shaped domains. For rapid cooling

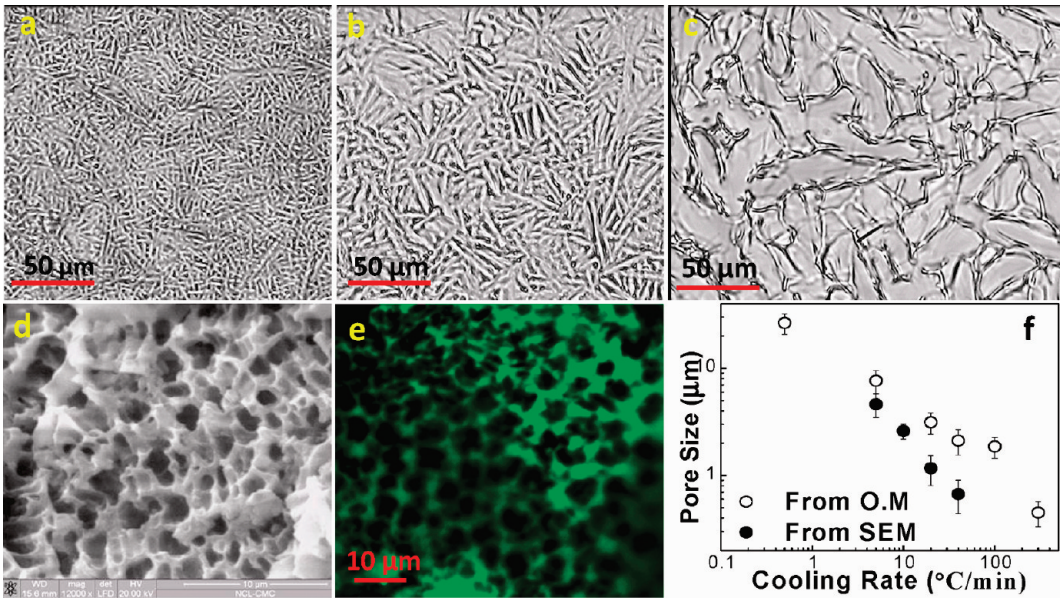

Figure 2. Optical micrographs of cross-linked network structures formed from assembly of 15 nm Si−PEI particles (5 wt %), at the domain boundaries of the H_1 phase at cooling rates of (a) 10, (b) 5, and (c) 0.5 °C/min. As the cooling rate is increased, we observe a decrease in the domain size. (d) SEM micrograph of self-standing scaffold prepared at a cooling rate of 10 °C/min. (e) Confocal micrograph image of cross-linked self-standing scaffold, tagged with a green dye, fluorescein isothiocyanate (FITC), after removal of the surfactant template and imaged using an argon laser at an excitation wavelength of 488 nm. The scaffold was formed by cooling 15 nm Si−PEI particles in the H_1 phase at 5 °C/min. (f) Decrease in pore size (from optical micrographs and SEM) observed as a function of cooling rate. The error bars represent the standard deviation over multiple measurements as indicated in the main text.

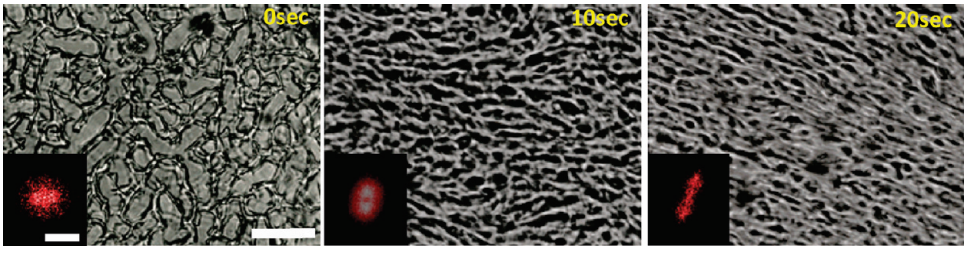

Figure 3. Optical micrographs of cross-linked networks of PEI-coated 15 nm silica particles (5 wt %) assembled by cooling at 0.5 °C/min from the isotropic dispersed phase to room temperature and then sheared at 0.01 s^{-1} for (a) 0, (b) 10, and (c) 20 s. The scale bar indicated represents 50 μm. The inset shows the Fourier transform of the optical microscopy images, and the scale bar corresponds to 2.6 μm^{-1}.

rates (>5 °C/min), where dense nucleation precludes extensive domain growth before impingement, the final domain morphology (and therefore, particle organization in the particle−H_1 composite) is determined by the elongated shapes of the initially developed bâtonnets.

We observe that the elongated shape of the particle assembly is not retained after cross-linking and surfactant removal, when the final macroporous solid is imaged using SEM (Figure 1d and e, Figure 2d; also see the Supporting Information) and confocal microscopy (Figure 2e). While the anisotropic shape of the pores in the network are not retained after surfactant removal, the decrease in average pore size in the free-standing macroporous solid with cooling rate is preserved and correlates with the decrease in mesh width in the particle−surfactant composite (Figure 2f). Thus, while the cross-linked particulate mesh of coated silica particles has sufficient mechanical stability to retain macroporosity after surfactant removal, and even on drying, it is unable to retain the elongated domain shapes observed in the particle−surfactant composite.

The particulate network/H_1 system is a gel that can be readily restructured and oriented by application of shear (Figure 3). Shearing of H_1 gels results in orientation of the surfactant cylinders along the flow direction at low shear rates and in shear melting at higher rates.[33] In polydomain samples, there is yielding as shear aligns the various domains, and eventually, a monodomain forms. In our Si-PEI/H_1 systems, shearing at a rate of 0.01 s^{-1} results in progressive flow-direction alignment of the particulate strands and a concomitant decrease in the strand−strand spacing with increasing strain units (Figure 3). Fourier transforms of the optical micrographs (insets) clearly indicate an increase in flow-direction alignment, with increasing strain. We note that extensional flow, imposed, for example, by squeezing the particle/H_1 gel through a syringe with a tapered exit, also efficiently orients the particle networks. In all flow-orientation experiments, the glutaraldehyde cross-linker concentrations are adjusted so that the orientation is complete at time scales significantly shorter than that required for extensive cross-linking. We have also applied a similar shearing protocol on

dx.doi.org/10.1021/cm102945x |*Chem. Mater.* 2011, 23, 1448–1455

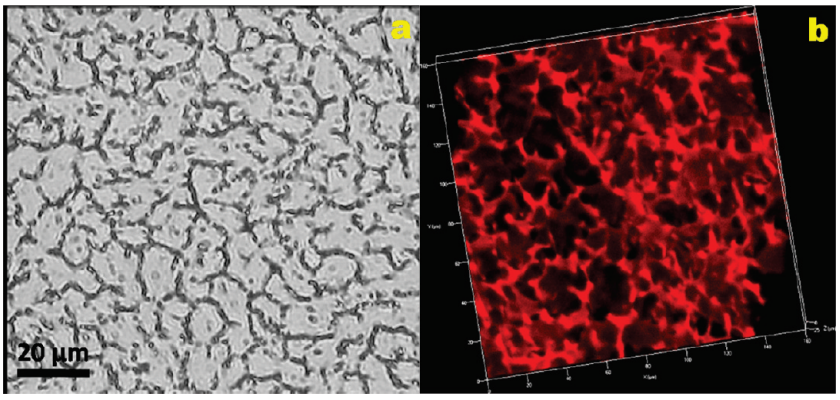

Figure 4. (a) Optical micrograph of a network of PEI-coated hydroxyapatite particles (HAP). (b) Laser scanning confocal micrograph (514 nm filter) showing 3D image of 120 × 120 × 25 μm self-standing HAP scaffold. The scaffold is functionalized with biotin, and the biotin functionalized network is incubated with fluorescent streptavidin-phycoerythrin and imaged using confocal.

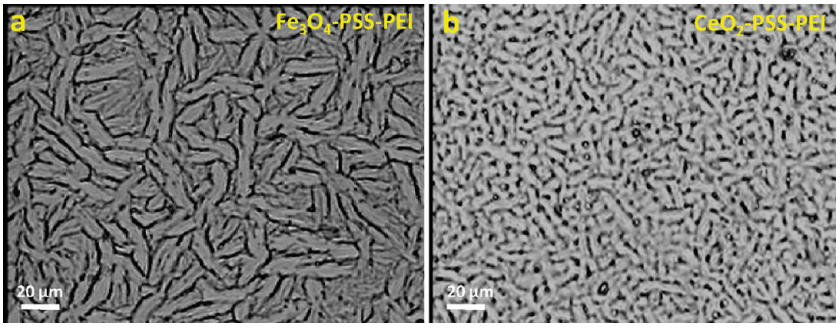

Figure 5. Optical micrographs of self-assembled networks formed by positively charged particles: (a) Fe_3O_4 particles and (b) Ceria particles.

self-assembled 978 nm PS-red particles in the H_1 phase, that can be observed using confocal microscopy. Confocal microscopy reveals the formation of a highly oriented structure comprised of interconnected particulate strands (see the Supporting Information).

Network formation by segregation of nanoparticles is observed to be independent of particle chemistry. Here, we describe preparation of self-supporting macroporous solids from dispersions of other inorganic nanoparticles. For example, PEI-coated hydroxyapatite particles (HAP), in $C_{12}E_9$—water assembled into a network by cooling at 5 °C/min and by subsequent cross-linking using glutaraldehyde as seen in the optical micrograph in Figure 4a. This material showed a mesh spacing of 20 μm, comparable to the minimum dimensions required for mammalian cell growth.[34] Materials with larger pore sizes can be prepared by slower cooling. Interestingly, as not all amine groups in the PEI react with glutaraldehyde, the strands of the macroporous solid are amenable to chemical modification. Such modification would be advantageous, for example, to graft cell adhesion promoters in scaffolds for cell growth. To demonstrate the possibility of chemical modification, the amine groups of PEI were further reacted with a biotin-NHS. The presence of the biotin on the scaffold was then probed using fluorescently labeled streptavidin, a tetrameric protein, which has a very high binding affinity for biotin. The biotin modified macroporous scaffold upon incubation with streptavidin-phycoerythrin turned fluorescent and could be imaged using confocal microscopy (Figure 4b). Control samples of scaffolds not treated with biotin-NHS did not show significant fluorescence. Thus, these macroporous materials allow diffusion of reactants through them and allow on-demand surface functionalization through the amine groups.

Inorganic nanoparticles with a positive surface charge can also be assembled into macroporous materials in the H_1 phase—in this case, we adopt the layer-by-layer technique to initially coat the nanoparticles with a polyanion (sodium salt of polystyrene sulfonate), followed by PEI. We have assembled cross-linked macroporous materials from 16 nm Fe_3O_4 magnetite particles, prepared with a positive surface charge to demonstrate this (Figure 5a). Similarly, positively charged ceria particles were coated with PSS and PEI and were also observed to assemble to form a network of strands in the surfactant H_1 phase (Figure 5b).

This methodology was also extended to form cross-linked three-dimensional networks from soft organic microparticles, such as polymer latices and proteins. We demonstrate assembly of 220 nm microgel particles of a temperature responsive polymer, PNIPAM in the H_1 phase. PEI-coated PNIPAM particles were cooled in aqueous surfactant solutions at 5 °C and were observed to assemble into networks as the surfactant H_1 phase formed. Interconnected strands of cross-linked PNIPAM microgel particles are seen in optical microscopy (Figure 6a). The PNIPAM microgel networks are self-standing after removal of the surfactant template and could be imaged using confocal microscopy after incubation with 10 ppm of rhodamine red dye for 24 h (Figure 6b). Such PNIPAM microgel networks are anticipated to have applications where relatively rapid volume transition kinetics are important,[35] as well as in sensing[36] and for drug delivery.[36] We note here, that we have also previously reported[37] the phase separation of PNIPAM linear chains to H_1 domain boundaries.

dx.doi.org/10.1021/cm102945x |*Chem. Mater.* 2011, 23, 1448–1455

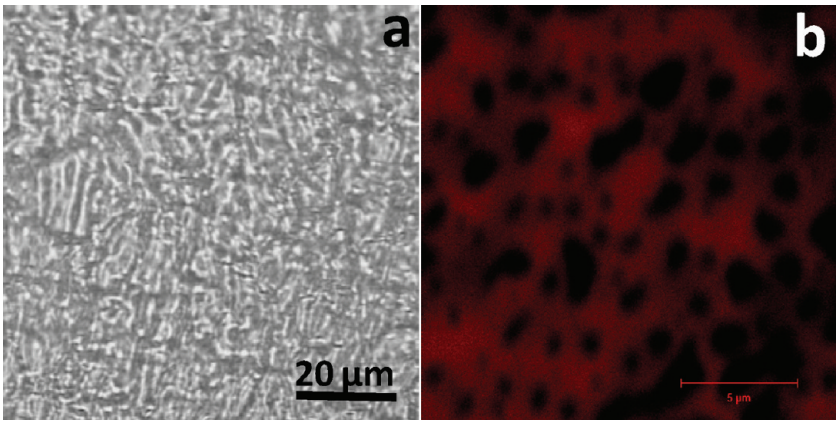

Figure 6. Self-standing network of 220 nm PEI-coated PNIPAM microgel particles cross-linked with glutaraldehyde. (a) Optical micrograph of the self-standing scaffold of PNIPAM in water, after the removal of surfactant. (b) 2D confocal micrograph of rhodamine tagged PNIPAM−PEI microgel network.

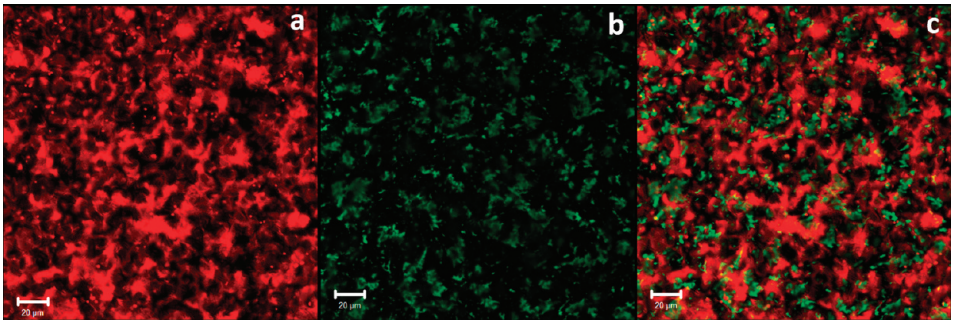

Figure 7. Confocal microscopy images of the interpenetrating structure formed by two different fluorescent PS particles (978 nm PS-Red and 490 nm PS-Green). (a) Structure formed by PS-Red on cooling at 0.5 °C in the H_1 phase. (b) Structure formed by PS-Green within the initially formed red particle structure. (c) Composite interpenetrating structure of PS-Green network within the PS-Red network. The scale bar in all images is 20 μm.

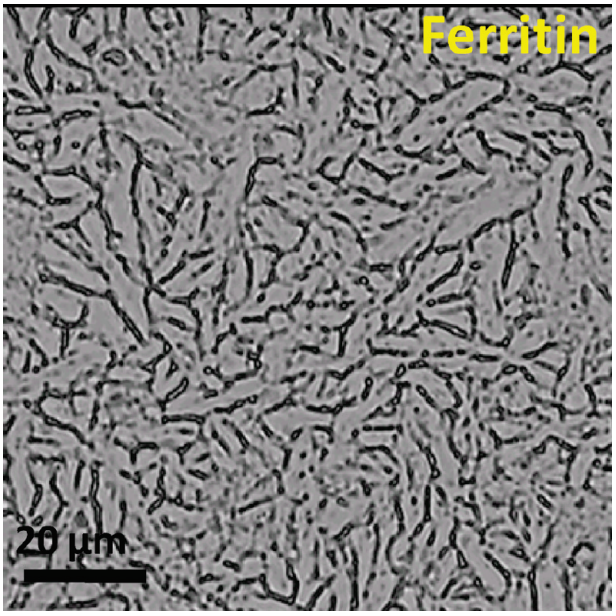

Figure 8. Optical micrograph of a network of ferritin, after cross-linking with glutaraldehyde.

Interpenetrating particle networks can also be formed using a two-step variation of this technique. We have assembled red fluorescently labeled 978 nm PS particles into a network on cooling at 0.5 °C/min. Subsequently, networks of a green fluorescently labeled 490 nm polystyrene (PS) particle were assembled from dispersions in the H_1 phase, by cooling at 5 °C/min, within the previously assembled network of red fluorescent particles (Figure 7c). Confocal microscopy indicates that each of the red and green fluorescent PS particles form an interconnected network (Figures 7a and b).

Finally, we tested this methodology to synthesize macroporous materials from a 450 kDa globular protein, ferritin. This bionanoparticle contains an iron oxide core within an assembly of 24 protein subunits. Assembly of such bionanoparticles into three-dimensional networks is still very challenging,[38] and chemical modification of the ferritin surface is typically necessary for assembly into networks. We demonstrate that native horse spleen ferritin can be organized into networks by dispersion in the surfactant H_1 phase. We cross-linked surface amine groups on the ferritin with glutaraldehyde to form a network that is stable in water, after template removal (Figure 8). Since different inorganic materials can be incorporated by using biomineralization into the core of ferritin from which the iron oxide core has been removed, this offers a route to develop macroporous scaffolds with unique functionalities.

SUMMARY

We demonstrate that dynamic phase separation of nonionic surfactant hexagonal domains is a generic technique for assembly of three-dimensional nanoparticulate networks. Inorganic, organic,

dx.doi.org/10.1021/cm102945x |*Chem. Mater.* 2011, 23, 1448–1455

and protein particles can be assembled into networks. The large surfactant content in solution renders the matrix amphiphilic, and therefore, hydrophobic nanoparticles can also be dispersed in such matrices.[23d] Dynamic templating of H_1 mesophases involves mild conditions—near ambient temperatures and a facile water wash for template removal. Thus, we demonstrate that it is possible to employ our technique to prepare networks of even relatively delicate bionanoparticles, such as ferritin protein, that would aggregate irreversibly on freezing. We believe that materials prepared using this technique have potential for application in a wide variety of technologically important areas.

■ ASSOCIATED CONTENT

Supporting Information. Particle synthesis, particle characterizations, formation of self-standing scaffolds from the particles mentioned in the study, and the characterization of the scaffolds.This material is available free of charge via the Internet at http://pubs.acs.org.

■ AUTHOR INFORMATION

Corresponding Author

*Tel.: +91-20-2590-2182. Fax: +91-20-2590-2618. E-mail: g.kumaraswamy@ncl.res.in (G.K.). Tel.: +91-20-2590-2747. Fax: +91-20-2590-2618. E-mail: ss.sengupta@ncl.res.in (S.S.G.).

■ ACKNOWLEDGMENT

We are very grateful to E. Venugopal and Dr. Nandini Devi for preparing the iron oxide and ceria particles, respectively. The PNIPAM microgel particles were synthesized by Samruddhi Kamble. Samruddhi Kamble and V. J. Jijo performed initial experiments on assembly of PNIPAM microgels in the hexagonal mesophase. We thank Dr. Beena Pillai (IGIB, New Delhi) for providing us streptavidin-phycoerythrin conjugate. K.P.S. and A.K.G. acknowledge research fellowships from CSIR, New Delhi. S.S.G. acknowledges funding from the DST via grant number grant no. SR/S1/PC-56/2008.

■ REFERENCES

(1) Mann, S. *Nat. Mater.* **2009**, *8*, 781–792.

(2) (a) Iskandar, F.; Mikrajuddin; Okuyama, K. *Nano Lett.* **2001**, *1*, 231–234. (b) Vanbever, R.; Mintzes, J. D.; Wang, J.; Nice, J.; Chen, D.; Batycky, R.; Langer, R.; Edwards, D. A. *Pharm. Res.* **1999**, *16*, 1735–1742.

(3) Boal, A. K.; Ilhan, F.; DeRouchey, J. E.; Thurn-Albrecht, T.; Russell, T. P.; Rotello, V. M. *Nature* **2000**, *404*, 746–748.

(4) Lin, S.; Li, M.; Dujardin, E.; Girard, C.; Mann, S. *Adv. Mater.* **2005**, *17*, 2553–2559.

(5) Arachchige, I. U.; Brock, S. L. *Acc. Chem. Res.* **2007**, *40*, 801–810.

(6) Michna, S.; Wu, W.; Lewis, J. A. *Biomaterials* **2005**, *26*, 5632–5639.

(7) Davis, S. A.; Breulmann, M.; Rhodes, K. H.; Zhang, B.; Mann, S. *Chem. Mater.* **2001**, *13*, 3218–3226.

(8) Nie, Z.; Petukhova, A.; Kumacheva, E. *Nature Nanotechnol.* **2009**, *5*, 15–25.

(9) (a) Vlasov, Y. A.; Yao, N.; Norris, D. *J. Adv. Mater.* **1999**, *11*, 165–169. (b) Velev, O. D.; Kaler, E. W. *Adv. Mater.* **2000**, *12*, 531–534. (c) Rhodes, K. H.; Davis, S. A.; Caruso, F.; Zhang, B.; Mann, S. *Chem. Mater.* **2000**, *12*, 2832–2834. (d) Stein, A.; Li, F.; Denny, N. R. *Chem. Mater.* **2007**, *20*, 649–666.

(10) (a) Caruso, R. A.; Antonietti, M. *Chem. Mater.* **2001**, *13*, 3272–3282. (b) Wang, Y.; Tang, Y.; Dong, A.; Wang, X.; Ren, N.; Shan, W.; Gao, Z. *Adv. Mater.* **2002**, *14*, 994–997.

(11) (a) Breulmann, M.; Davis, S. A.; Mann, S.; Hentze, H. P.; Antonietti, M. *Adv. Mater.* **2000**, *12*, 502–507. (b) Caruso, R. A.; Giersig, M.; Willig, F.; Antonietti, M. *Langmuir* **1998**, *14*, 6333–6336.

(12) (a) Huerta, L.; Guillem, C.; Latorre, J.; Beltrán, A.; Beltrán, D.; Amorós, P. *Chem. Commun.* **2003**, 1448–1449. (b) Zhang, Y.; Zha, S.; Liu, M. *Adv. Mater.* **2005**, *17*, 487–491.

(13) Davis, S. A.; Patel, H. M.; Mayes, E. L.; Mendelson, N. H.; Franco, G.; Mann, S. *Chem. Mater.* **1998**, *10*, 2516–2524.

(14) (a) Böker, A.; Lin, Y.; Chiapperini, K.; Horowitz, R.; Thompson, M.; Carreon, V.; Xu, T.; Abetz, C.; Skaff, H.; Dinsmore, A. D.; Emrick, T.; Russell, T. P. *Nat. Mater.* **2004**, *3*, 302–306. (b) Bunz, U. H. F. *Adv. Mater.* **2006**, *18*, 973–989. (c) Sakatani, Y.; Boissière, C.; Grosso, D.; Nicole, L.; Soler-Illia, G. J. A. A.; Sanchez, C. *Chem. Mater.* **2007**, *20*, 1049–1056. (d) Shah, P. S.; Sigman, M. B., Jr.; Stowell, C. A.; Lim, K. T.; Johnston, K. P.; Korgel, B. A. *Adv. Mater.* **2003**, *15*, 971–974.

(15) (a) Walsh, D.; Arcelli, L.; Ikoma, T.; Tanaka, J.; Mann, S. *Nat. Mater.* **2003**, *2*, 386–390. (b) Wu, M.; Fujiu, T.; Messing, G. L. *J. Non-Cryst. Solids* **1990**, *121*, 407–412. (c) Walsh, D.; Kulak, A.; Aoki, K.; Ikoma, T.; Tanaka, J.; Mann, S. *Angew. Chem., Int. Ed.* **2004**, *43*, 6691–6695.

(16) Lin, Y.; Skaff, H.; Emrick, T.; Dinsmore, A. D.; Russell, T. P. *Science* **2003**, *299*, 226–229.

(17) (a) Herzig, E. M.; White, K. A.; Schofield, A. B.; Poon, W. C. K.; Clegg, P. S. *Nat. Mater.* **2007**, *6*, 966–971. (b) Stratford, K.; Adhikari, R.; Pagonabarraga, I.; Desplat, J.-C.; Cates, M. E. *Science* **2005**, *309*, 2198–2201.

(18) (a) Zhang, H.; Hussain, I.; Brust, M.; Butler, M. F.; Rannard, S. P.; Cooper, A. I. *Nat. Mater.* **2005**, *4*, 787–793. (b) Munch, E.; Launey, M. E.; Alsem, D. H.; Saiz, E.; Tomsia, A. P.; Ritchie, R. O. *Science* **2008**, *322*, 1516–1520. (c) Deville, S.; Saiz, E.; Nalla, R. K.; Tomsia, A. P. *Science* **2006**, *311*, 515–518. (d) Vickery, J. L.; Patil, A. J.; Mann, S. *Adv. Mater.* **2009**, *21*, 2180–2184.

(19) (a) Anderson, V. J.; Terentjev, E. M.; Meeker, S. P.; Crain, J.; Poon, W. C. K. *Eur. Phys. J. E.* **2001**, *4*, 11–20. (b) Meeker, S. P.; Poon, W. C. K.; Crain, J.; Terentjev, E. M. *Phys. Rev. E* **2000**, *61*, R6083. (c) Petrov, P. G.; Terentjev, E. M. *Langmuir* **2001**, *17*, 2942–2949. (d) West, J. L.; Glushchenko, A.; Liao, G.; Reznikov, Y.; Andrienko, D.; Allen, M. P. *Phys. Rev. E* **2002**, *66*, 012702. (e) Vollmer, D.; Hinze, G.; Poon, W. C. K.; Cleaver, J.; Cates, M. E. *J. Phys.: Condens. Matter* **2004**, *16*, L227–L233.

(20) (a) Poulin, P.; Raghunathan, V. A.; Richetti, P.; Roux, D. *J. Phys. II France* **1994**, *4*, 1557–1569. (b) Ramaswamy, S.; Nityananda, R.; Raghunathan, V. A.; Prost, J. *J. Mol. Cryst. Liq. Cryst.* **1998**, *288*, 175–180. (c) Poulin, P.; Francès, N.; Mondain-Monval, O. *Phys. Rev. E* **1999**, *59*, 4384–4387. (d) Loudet, J. C.; Barois, P.; Auroy, P.; Keller, P.; Richard, H.; Poulin, P. *Langmuir* **2004**, *20*, 11336–11347. (e) Muševič, I.; Škarabot, M.; Tkalec, U.; Ravnik, M.; Žumer, S. *Science* **2006**, *313*, 954–958.

(21) (a) Basappa, G.; Suneel; Kumaran, V.; Nott, P. R.; Ramaswamy, S.; Naik, V. M.; Rout, D. *Eur. Phys. J. B* **1999**, *12*, 269–276. (b) Zapotocky, M.; Ramos, L.; Poulin, P.; Lubensky, T. C.; Weitz, D. A. *Science* **1999**, *283*, 209–212.

(22) Sharma, K. P.; Kumaraswamy, G.; Ly, I.; Mondain-Monval, O. *J. Phys. Chem. B* **2009**, *113*, 3423–3430.

(23) (a) Fabre, P.; Casagrande, C.; Veyssie, M.; Cabuil, V.; Massart, R. *Phys. Rev. Lett.* **1990**, *64*, 539–542. (b) Quilliet, C.; Ponsinet, V.; Cabuil, V. *J. Phys. Chem.* **1994**, *98*, 3566–3569. (c) Alexeev, V. L.; Ilekti, P.; Persello, J.; Lambard, J.; Gulik, T.; Cabane, B. *Langmuir* **1996**, *12*, 2392–2401. (d) Eiser, E.; Bouchama, F.; Thathagar, M. B.; Rothenberg, G. *ChemPhysChem* **2003**, *4*, 526–528. (e) Ramos, L.; Fabre, P.; Nallet, F.; Lu, C.-Y. D *Eur. Phys. J. E.* **2000**, *1*, 285–299. (f) Bouchama, F.; Thathagar, M. B.; Rothenberg, G.; Turkenburg, D. H.; Eiser, E. *Langmuir* **2004**, *20*, 477–483.

(24) Sharma, K. P.; Aswal, V. K.; Kumaraswamy, G. *J. Phys. Chem. B* **2010**, *114*, 10986–10994.

(25) Wadekar, M. N.; Pasricha, R.; Gaikwad, A. B.; Kumaraswamy, G. *Chem. Mater.* **2005**, *17*, 2460.
(26) Chandran, S. P.; Hotha, S.; Prasad, B. L. V. *Curr. Sci.* **2008**, *95*, 1327.
(27) Senff, H.; Richtering, W. *Colloid Polym. Sci.* **2000**, *278*, 830.
(28) Iida, H.; Takayanagi, K.; Nakanishi, T.; Osaka, T. *J. Colloid Interface Sci.* **2007**, *314*, 274.
(29) Yuan, Z,-Y; Idakiev, V.; Vantomme, A.; Tabakova, T.; Ren, T.,-Z.; Su, B.,-L. *Catal. Today* **2008**, *131*, 203.
(30) Bringley, J. F.; Wunder, A.; Howe, A. M.; Wesley, R. D.; Qiao, T. A.; Liebert, N. B.; Kelley, B.; Minter, J.; Antalek, B.; Hewitt, J. M. *Langmuir* **2006**, *22*, 4198–4207.
(31) Knight, P.; Wyn-Jones, E.; Tiddy, G. J. T. *J. Phys. Chem.* **1985**, *89*, 3447–3449.
(32) *Textures of Liquid Crystals*; Dierking, I., Ed.; Wiley-VCH: New York, 2003.
(33) (a) Ramos, L.; Molino, F.; Porte, G. *Langmuir* **2000**, *16*, 5846–5848. (b) Schmidt, G.; Muller, S.; Lindner, P.; Schmidt, C.; Richtering, W. *J. Phys. Chem. B* **1998**, *102*, 507–513.
(34) Freyman, T. M.; Yannas, I. V.; Gibson, L. J. *Prog. Mater. Sci.* **2001**, *46*, 273–282.
(35) Cho, E. C.; Kim, J.-W.; Fernandez-Nieves, A.; Weitz, D. A. *Nano Lett.* **2007**, *8* (1), 168–172.
(36) (a) Zhang, Y.; Guan, Y.; Zhou, S. *Biomacromolecules* **2007**, *7*, 3196–3201. (b) Hu, Z.; Huang, G. *Angew. Chem., Int. Ed.* **2003**, *42*, 4799–4802. (c) Kim, J.; Nayak, S.; Lyon, L. A. *J. Am. Chem. Soc.* **2005**, *127*, 9588–9592.
(37) Jijo, V. J.; Sharma, K. P.; Mathew, R.; Kamble, S.; Rajamohanan, P. R.; Ajithkumar, T. G.; Badiger, M. V.; Kumaraswamy, G. *Macromolecules* **2010**, *43*, 4782–4790.
(38) (a) Broomell, C. C.; Birkedal, H.; Oliveira, C. L. P.; Pedersen, J. S.; Gertenbach, J. A.; Young, M.; Douglas, T. *Soft Matter* **2010**, *6*, 3167–3171. (b) Hu, Y.; Chen, D.; Park, S.; Emrick, T.; Russell, T. P. *Adv. Mater.* **2010**, *22*, 2583–2587.